Effect of cell surfaces on the stability of chiral smectic-*C* phases

U. Manna, Jang-Kun Song, G. Power, and J. K. Vij*
Department of Electronic and Electrical Engineering, Trinity College, University of Dublin, Dublin, Ireland
(Received 13 December 2007; revised manuscript received 17 May 2008; published 27 August 2008)

The effect of surfaces on the stability of smectic-C^* (SmC^*) variant phases is investigated. The results obtained using dielectric spectroscopy by varying the cell thickness show that the temperature ranges of SmC^*_α, Sm$C^*_A(1/2)$, and Sm$C^*_A(1/3)$ phases decrease with decreasing cell thickness, and the Sm$C^*_A(1/3)$ phase is more stable than the Sm$C^*_A(1/2)$ phase. The relative stability of any phase is found to be due to its large polar anchoring strength and low free energy compared to other phases in a cell. Experimental results are found to agree with the theory.

DOI: 10.1103/PhysRevE.78.021711 PACS number(s): 61.30.Hn, 64.70.M−, 77.22.Gm

I. INTRODUCTION

Chandani *et al.* [1,2] discovered antiferroelectric (AF) liquid crystals and in particular they discovered the three smectic-C^* (SmC^*) phases SmC^*_A, SmC^*_α, and SmC^*_γ in 1989. The other phase involving four-layer periodicity with almost zero spontaneous polarization, called AF, was discovered by Okabe *et al.* [3]. Gorecka *et al.* [4] and Takezoe *et al.* [5] proposed models for the SmC^*_γ and AF phases and gave the periodicity of the layers as 3 and 4, respectively. Recently, Chandani *et al.* [6] also discovered a subphase involving a five-layer periodicity sandwiched between the two- and three-layer phases. The latter exists over a narrow range of temperatures and was confirmed independently by Panov *et al.* [7] using a different optical technique. Several theoretical approaches have been considered to explain a variety of these phases based on the Landau model [8,9], namely, the Ising [10], clock [11], distorted clock [12,13], and discrete flexoelectric models [14,15]. The SmC^* phase is a tilted phase with the director tilted from the layer normal; each layer has a spontaneous polarization directed normal to the plane formed by the director and the layer normal. Due to the chirality a helical structure is formed. Application of an electric field aligns the spontaneous polarization of each layer of the SmC^* phase along the field, which creates a large induced macroscopic polarization. The SmC^*_α phase has a helical structure as well, but the pitch is extremely short. The structure of the SmC^*_α phase is obtained by minimizing the free energy of a system containing competing interactions between the nearest and the next-nearest smectic layers and by assuming the temperature dependence of the tilt angle [15,16]. We use the nomenclature of the liquid crystalline phases introduced first by Isozaki *et al.* [17] for the reason that the arrangement of the fraction of ferroelectric order in a unit cell is explicitly specified. Isozaki *et al.* defined the various phases as $q_T=[F]/([A]+[F])$, where $[F]$ and $[A]$ are the amounts of ferroelectric and antiferroelectric orderings in a unit cell. Since all of these phases are closely related to SmC^*_A, they designated them as Sm$C^*_A(q_T)$. Thus Sm$C^*_A(0)$, Sm$C^*_A(1/3)$, and Sm$C^*_A(1/2)$ are the designations for a two-layer, three-layer (also called SmC^*_γ and SmC^*_{FI1} by different groups), and four-layer (called AF or SmC^*_{FI2}) phase, respectively. The advantage of using the Isozaki *et al.* [17] notation is that any newly discovered phase can be accommodated within the scheme and the number of layers in a unit cell readily calculated, whereas the other numbered designations may be misleading. Furthermore, SmC^*_{FI2} is an antiferroelectric phase rather than a ferrielectric phase as may be implied by this nomenclature.

Liquid crystal devices exploit the phenomenon of alignment by surfaces [18]. It has been known for some time that the phase transitions of chiral smectic liquid crystals are controlled by their confinement [19–27] and by their alignment [28]. The results of dielectric spectroscopy and optical texture experiments have been used to compare the antiferroelectric liquid crystal (AFLC) phase behaviors of several compounds confined in cells of different thicknesses [19–21]. Electro-optical and dielectric spectroscopic investigations performed at several different cell gaps on three homologs of the series *n*OF1M7, where *n* denotes the length of the unbranched terminal chain, showed that the bulk thermodynamic phase existed only in samples of cell thicknesses greater than 25 μm. It was found that the Sm$C^*_A(1/3)$-SmC^*_A transition temperature was pushed downward as the measurement cell gap was reduced for thin cells. For a thin cell, the SmC^*_A phase completely disappeared and the coexistence of ferroelectric and antiferroelectric phases was observed [22]. It was also found that confinement of AFLCs induces a phase transformation from the Sm$C^*_A(1/2)$ and Sm$C^*_A(1/3)$ phases to the frustrated ferroelectric SmC^* phase, which showed thresholdless bistable switching [23]. The transition temperature of the Sm*A*-SmC^* transition is found to be lowered and the ferrielectric phases are suppressed in pores of nanometer dimensions of liquid crystalline phases in porous media [24]. The second-order transition from Sm*A* to SmC^* is considerably broadened and an additional relaxation process is detected for liquid crystals confined in aerogel pores [25]. Thinner cells exhibit more field-induced ferrielectric steps in optical transmission than do thicker cells [26].

Nevertheless, results on the transition temperatures and temperature ranges of SmC^* variant phases have not so far been obtained systematically as a function of the cell thickness, nor explained by a theory that determines the stability of these phases. This approach may also be applicable to

*jvij@tcd.ie

other areas of surface science. We theoretically analyze the effect of surfaces on the stability of these phases by considering the contribution of the surface anchoring energy and the distortion energy of the bulk liquid crystals contributed by the surfaces to clarify how the transition temperatures depend on the cell thickness and why the temperature range of some of the phases decreases rapidly with decreasing cell thickness. Finally, some of the phases are not observed for low cell thicknesses. We present experimental data on the variation of the transition temperatures and temperature ranges of the SmC^* variant phases of a prototype AFLC compound as a function of the cell thickness in the range 3–80 μm. The experimental results also give the extent of the order of the suppression and the nature of the stability of the smectic-C^* variant phases relative to each other. The experimental results are found to agree with the theory.

II. THEORY

Orihara and Ishibashi [8] in 1990 were the first to suggest a phenomenological model based on the Landau theory of phase transitions applied to the chiral smectic-C^* variant phases soon after their discovery. Since then, several phenomenological models have emerged [9–15] to explain the various experimental observations. Landau theory, which is a global method to describe phase transitions, is based on a few basic assumptions. One of these assumptions is that the free energy is analytical and at least one of the analytical terms contains the temperature T. The temperature-dependent term is selected to describe the phase transition phenomenologically. Therefore, despite a variety of phenomenological models based on the Landau description having been advanced to date, the basic terms in the models are quite similar. For example, the discrete flexoelectric model [14,15] given recently for explaining the emergence of possible phases or subphases uses a free energy equation as below:

$$VF_b = \sum_{i=1}^{N} \left(\tilde{F}_0(\theta) - \tilde{a}\frac{\Delta T}{T_C}(\cos\varphi_{i-1,i} + \cos\varphi_{i,i+1}) - \tilde{B}(\cos^2\varphi_{i-1,i} + \cos^2\varphi_{i,i+1}) + f(\mathbf{P}_{i-1},\mathbf{P}_i,\mathbf{P}_{i+1}) \right), \tag{1}$$

where F_b is the free energy per unit volume, V is the volume of the cell, and $i=1,\ldots,N$ is the running index of smectic layers for a cell having N layers. $\tilde{F}_0(\theta)$ is the tilt-angle (θ) dependent free energy part that governs the nontilted to tilted phase transition, that is, the SmA^*-SmC^* phase transition. φ is defined as the angle that the **c** director of a layer makes with the x direction on the cell window as shown in Fig. 1(b). The second and third terms are designed to express the synclinic to anticlinic phase transition, that is, the ferrro-to antiferroelectric layer ordering transition. $\Delta T = T - T_C$, where T_C is the transition temperature between the synclinic and anticlinic smectic-C^* phases in the absence of any intermediate phases. The second term is temperature dependent, while the other terms are temperature independent. The last term in Eq. (1) is a function of the polarization **P**, which was introduced by Osipov *et al.* [15], to explain the emergence of the various phases and subphases. The last term is dependent on the model and can be controversial (this is not explained in detail here because it is beyond the scope of our paper). The first three terms, however, have a clear physical meaning and these appear in slightly different forms in almost all of the phenomenological models based on the Landau free energy expansion. The in-layer molecular directors for the synclinic or anticlinic orderings almost lie in a single plane for positive $\tilde{B}$. As the temperature increases, the ferroelectric configuration is favored by positive $\tilde{a}$. Equation (1) can be rewritten as

$$F_b = T\frac{1}{V}\sum_{i=1}^{N}\left(-\tilde{a}\frac{1}{T_C}(\cos\varphi_{i-1,i} + \cos\varphi_{i,i+1})\right) + \frac{1}{V}\sum_{i=1}^{N}[\tilde{F}_0(\theta) + \tilde{a}(\cos\varphi_{i-1,i} + \cos\varphi_{i,i+1}) - \tilde{B}(\cos^2\varphi_{i-1,i} + \cos^2\varphi_{i,i+1}) + f(\mathbf{P}_{i-1},\mathbf{P}_i,\mathbf{P}_{i+1})]. \tag{2}$$

Now Eq. (2) can be rewritten as

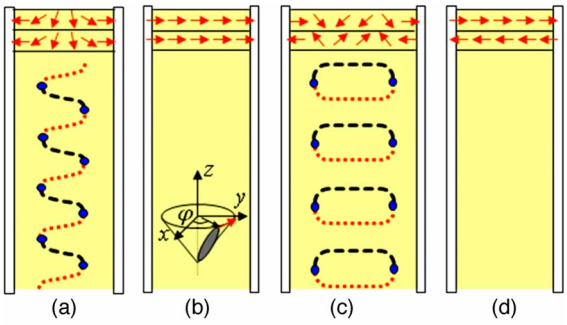

FIG. 1. (Color online) Schematic for the director distribution in SmC^* variant phases based on the works of Brunet [30] and Glogarova [31]. Director distribution of the SmC^* phase for a thick (a) and for a thin (b) cell, where the number of layers with $\varphi=0$ and $\varphi=\pi$ is not the same in the unwound state, resulting in a nonzero spontaneous polarization. The red arrows in the upper part represent the spontaneous polarization along the y direction for the first two layers (twist structure), black round dotted and red square dotted lines in the center denote the directors having $\bar{\varphi}=\pi/2$ and $-\pi/2$, respectively, and blue circles denote defects. The director distribution in the Sm$C_A^*(1/3)$ phase follows the same distribution as in (a) and (b) for thick and thin cells, respectively, except the director of the third layer is opposite to that of the first two layers. Director distribution in SmC_A^* phase for a thick (c) and thin (d) cell, where the number of layers of $\varphi=0$ is the same as of $\varphi=\pi$ in the unwound state, resulting in zero spontaneous polarization. The director distribution of the Sm$C_A^*(1/2)$ phase follows the same distribution as in (c) and (d) for thick and thin cells, respectively, except the repeating unit has four layers. The defects in (a) and (c) induced by the helical structure disappear in a thin cell. For larger cell thicknesses, the twist structure in (a) coexists with the helical structure, whereas for intermediate cell thicknesses only the twist structure exists.

$$F_b = T\left\langle -\frac{\tilde{a}}{T_C}(\cos\varphi_{i-1,i} + \cos\varphi_{i,i+1})\right\rangle + F_O \equiv AT + F_O, \tag{3}$$

where $A \equiv -(\tilde{a}/T_C)\langle\cos\varphi_{i-1,i}+\cos\varphi_{i,i+1}\rangle \equiv -A_O\langle\cos\varphi_{i-1,i}+\cos\varphi_{i,i+1}\rangle$. $\langle\,\rangle$ denotes the average temperature dependent free energy term per unit volume, and replaces the summation in Eq. (2). Here, F_O denotes the sum of all the other terms in Eq. (2) per unit volume and is independent of temperature and dependent on the structure, polarization, etc. With a cell having surface area S and thickness d, the total free energy can be written as

$$F_T = SdF_b + 2SF_s, \tag{4}$$

$$F_T/Sd \equiv F_t = F_b + 2F_s/d. \tag{5}$$

Here, F_s is the free energy contributed by the unit surface. This includes the anchoring energy and the distortion energy of the bulk liquid crystals contributed by the surfaces. Hence, we get $F_t = AT + F_O + 2F_s/d$. Here, since we are considering a small shift in the phase transition temperatures due to the surface effect, F_s is considered to be independent of temperature for a narrow range of temperatures close to the phase transition temperature. We consider the phase transition between the phases 1 and 2 having $q_T = q_1$ (lower temperature) and $q_T = q_2$ (higher temperature) phases. At the bulk transition temperature T_C in the absence of the surfaces, the bulk free energies of two phases are the same. Hence,

$$A_{q1}T_C + F_{O,q1} = A_{q2}T_C + F_{O,q2}. \tag{6}$$

The transition temperature T, by including the surface effect, can be found as

$$A_{q1}T + F_{O,q1} + 2F_{s,q1}/d = A_{q2}T + F_{O,q2} + 2F_{s,q2}/d. \tag{7}$$

Hence, the transition temperature's dependence on the surfaces is given by

$$T = T_C - \frac{2(F_{s,q1} - F_{s,q2})}{d(A_{q1} - A_{q2})} = T_C - \frac{2\Delta F_{s,(q1,q2)}}{\Delta A_{q1,q2}}\frac{1}{d}. \tag{8}$$

We find from Eq. (8) that a shift in the transition temperature due to the surface interactions is inversely proportional to the cell thickness, and it depends on the ratio of the differences in the coefficient of the temperature-dependent term for the free energy (ΔA) and the surface energy (ΔF_s). The effect of surfaces can therefore be calculated using this equation. ΔA can be calculated using Eq. (3) and, if phase 1 is the lower-temperature phase, then ΔA is always positive. Hence the sign of the coefficient of the last term in Eq. (8) is determined by ΔF_s. If ΔF_s is positive, i.e., the surface energy of phase 1 is higher than that of phase 2, the transition temperature decreases with decreasing cell thickness. On the contrary, if ΔF_s is negative, that is, the surface energy of phase 1 is lower than that of phase 2, the transition temperature increases on decreasing the cell thickness.

The free energy parameter A can be found from Eq. (3) for the transitions among SmC^*, Sm$C_A^*(1/2)$, Sm$C_A^*(1/3)$, and SmC_A^* phases. However, for the transitions among SmA^*, SmC_α^*, and SmC^*, the first term in Eq. (1) contributes significantly to the phase transition. That is, close to the SmA^*-SmC^* transition, the tilt angle θ changes sharply with temperature, and the free energy is mostly governed by the tilt-angle-dependent term. Note that the Landau expansion for the second-order SmA^* to SmC^* transition is

$$F_{AC} = f_0 + a_0(T - T_{AC})\theta^2 + a_4\theta^4 + \cdots. \tag{9}$$

Thus, for the transitions among SmA^*, SmC_α^*, and SmC^*, $A \equiv a_0\theta^2$. Here, a_0 is the Landau coefficient of the temperature-dependent term. a_0 is much greater than $A_0 = \tilde{a}/T_C$, since the energy difference between SmA^* and SmC^* is 10^3 times that between SmC^* and SmC_A^* [15]; $\tilde{a}$ is the coefficient of the second term in Eq. (1). Therefore, in Eq. (8), ΔA for the transitions among SmA^*, SmC_α^*, and SmC^* is much higher than for those among SmC^*, Sm$C_A^*(1/2)$, Sm$C_A^*(1/3)$, and SmC_A^*. This means that the transition temperatures between SmA^*, SmC_α^*, and SmC^* phases are found to be largely insensitive to the cell thickness.

In order to calculate ΔF_s for the transitions among the variant SmC^* phases, we consider the surface energy F_s in detail. We assume that the phase transition occurs in the bulk liquid crystal as well as within the interface of the cell with the liquid crystal. The surface energy induces a distortion in the bulk LC. F_s can be separated into three different types of energy: the surface anchoring energy W_s, the distortion energy of the helix, $d\bar{\varphi}/dz$, and the in-layer distortion along the thickness direction, $d\bar{\varphi}/dy$. These energies are actually coupled to each other, and hence the total energy F_s written below can be calculated from the different components with justifiable approximations:

$$F_s = W_s + \frac{1}{S}\int\left[K_1\left(\frac{d\bar{\varphi}}{dz} - \bar{\varphi}_0\right)^2 + K_2\left(\frac{d\bar{\varphi}}{dy}\right)^2\right]dV. \tag{10}$$

$\bar{\varphi}$ is the azimuthal angle of the director of the last layer of a single period of the structure in each phase, i.e., $\bar{\varphi}$ is the angle of every fourth, third, and second layer in the Sm$C_A^*(1/2)$, Sm$C_A^*(1/3)$, and SmC_A^* phases, respectively. For SmC^*, $\bar{\varphi} = \varphi$. $\bar{\varphi}_0 = 2\pi/p$ (p is the pitch) is the wave vector. W_s can be written as [29]

$$W_s = -w_1\langle\cos\varphi_1 - \cos\varphi_2\rangle - w_2\langle\cos^2\varphi_1 + \cos^2\varphi_2\rangle, \tag{11}$$

where w_1 and w_2 are the polar and nonpolar coefficients of the anchoring energies, respectively, and φ_1 and φ_2 are the values of φ at surfaces 1 and 2, respectively. When w_2 is sufficiently large, φ_1 and φ_2 should be either 0 or π. $\langle\,\rangle$ in Eq. (11) denotes the average over the unit surface.

The director distributions for different cells with AFLCs in different phases based on the work [30,31] for SmC^* are plotted in Fig. 1. In the SmC_A^* and Sm$C_A^*(1/2)$ phases the number of layers of $\varphi = 0$ is the same as that of $\varphi = \pi$ in the unwound state, resulting in zero spontaneous polarization, whereas in the SmC^* and Sm$C_A^*(1/3)$ phases the number of layers with $\varphi = 0$ and $\varphi = \pi$ is not the same in the unwound state, resulting in nonzero spontaneous polarization. In the SmC_A^* and Sm$C_A^*(1/2)$ phases, W_s does not depend on

TABLE I. A and F_s for smectic-A^* and smectic-C^* variant phases. The upper part of the Table represents A and F_s for transitions among SmC*, $SmC_A^*(1/2)$, $SmC_A^*(1/3)$ and SmC_A^* phase, and the lower part of the Table represents A and F_s for transitions among SmA^*, SmC_α^* and SmC^* phases.

	A	$F_s(d<d_c,d_h)$	$F_s(d>d_c,d_h)$
SmC^*	$-2A_0$	$-2w_2+K_1\bar{\varphi}_{0,1}^2 d$	$-2(w_1+w_2)+d_hK_1\bar{\varphi}_{0,1}^2+\pi^2K_2/d$
$SmC_A^*(1/2)$	0	$-2w_2+K_1\bar{\varphi}_{0,1/2}^2 d$	$-2w_2+d_hK_1\bar{\varphi}_{0,1/2}^2$
$SmC_A^*(1/3)$	$2/3A_0$	$-2w_2+K_1\bar{\varphi}_{0,1/3}^2 d$	$-2/3w_1-2w_2+d_hK_1\bar{\varphi}_{0,1/3}^2+\pi^2K_2/d$
SmC_A^*	$2A_0$	$-2w_2+K_1\bar{\varphi}_{0,0}^2 d$	$-2w_2+d_hK_1\bar{\varphi}_{0,0}^2$
SmA^*	0		$-2w_2$
SmC_α^*	$a_0\theta_\alpha^2$		$-2w_2+d_hK_1\bar{\varphi}_{0,\alpha}$
SmC^*	$a_0\theta_{\text{ferro}}^2$	$-2w_2+K_1\bar{\varphi}_{0,1}^2 d$	$-2(w_1+w_2)+d_hK_1\bar{\varphi}_{0,1}^2+\pi^2K_2/d$

whether $\bar{\varphi}=0$ or π. However, in SmC^* and $SmC_A^*(1/3)$, it depends strongly on whether $\bar{\varphi}=0$ or π. When the thickness is large, the in-layer distortion energy is rather small, and consequently W_s is the most dominant term in F_s. So $\bar{\varphi}_1$ and $\bar{\varphi}_2$ are determined to have a minimum W_s; hence $\bar{\varphi}_1$ should be opposite to $\bar{\varphi}_2$ as shown in Fig. 1(a). However, when the thickness is low, the in-layer distortion energy increases, and in order to reduce F_s, as in Eq. (10), the in-layer distortion energy itself has to be reduced, in which case $\bar{\varphi}_1$ is the same as $\bar{\varphi}_2$, creating a uniform state as shown in Fig. 1(b). Thus, for the SmC^* and $SmC_A^*(1/3)$ phases, there exists a critical thickness d_c, for which W_s changes to reflect a sudden change from a twisted to a uniform state by a change in the direction of the director near one of the surfaces to reduce the in-layer distortion energy. The transition from the twist to the uniform alignment occurs when the anchoring energy difference between the two alignments becomes the same as the distortion energy of the twist. Approximately, it is found that $d_{c,1}=\pi^2K_2/(2w_1)$ for the SmC^* phase and $d_{c,1/3}=3\pi^2K_2/(2w_1)$ for the Sm$C^*(1/3)$ phase. Thus, $d_{c,1/3}$ is three times larger than $d_{c,1}$. However, for SmC^* and $SmC_A^*(1/2)$, W_s does not depend on the direction of $\bar{\varphi}$, so the minimum energy state is determined to have a minimum in-layer distortion energy for the entire range of thicknesses, as shown in Fig. 1(c), where $\bar{\varphi}_1=\bar{\varphi}_2$.

Now we consider the helical and the in-layer deformation energies. When the cell is thin, the in-layer distortion energy is too large to sustain the helical structure; hence the helical structures disappear and a uniform state is obtained. In the uniform state, the helical distortion energy becomes $K_1\bar{\varphi}_0^2 d$ per unit cell area from Eq. (10). As the cell thickness increases, a deformed helical structure appears from the center area and enlarges with increasing cell thickness. From this state, the helical distortion energy may not increase on increasing the cell thickness, since the helical structure in the center area has zero helical distortion energy. Therefore, the helical distortion energy for large cell thicknesses can be expressed as $K_1d_h\bar{\varphi}_0^2$, where d_h is another critical cell thickness indicating the change from the nonhelical to the helical structure. Based on this model, the calculated A and F_s for the different phases are listed in Table I. Usually typical domains in the surface stabilized ferroelectric cell, "up" and "down," appear approximately for 2–4 μm thickness in the SmC^* phase. For the SmC_α^* phase, $\bar{\varphi}_{0,\alpha}$ is very large, so F_s is mostly governed by $\bar{\varphi}_{0,\alpha}$. The period of pitch in SmC_α^* is just a few layers, while that in SmC^* is usually a few hundreds of layers. The results are calculated from the suggested model for simplified conditions: $d_{c,1}=2$ μm, $w_1/A_0=5.5\times10^6$ m, $a_0\theta_\alpha^2\sim1000A_0$, $a_0\theta_{\text{ferro}}^2\sim1300A_0$, $\bar{\varphi}_{0,\alpha}\sim50\bar{\varphi}_{0,1}$, $d_{h,1}=d_{h,0}=5$ μm, $d_{h,1/3}=d_{h,1/2}=100$ μm, $K_1\bar{\varphi}_{0,1}^2=K_1\bar{\varphi}_{0,0}^2=0.01w_1$, and $K_1\bar{\varphi}_{0,1/3}^2=K_1\bar{\varphi}_{0,1/2}^2=0$.

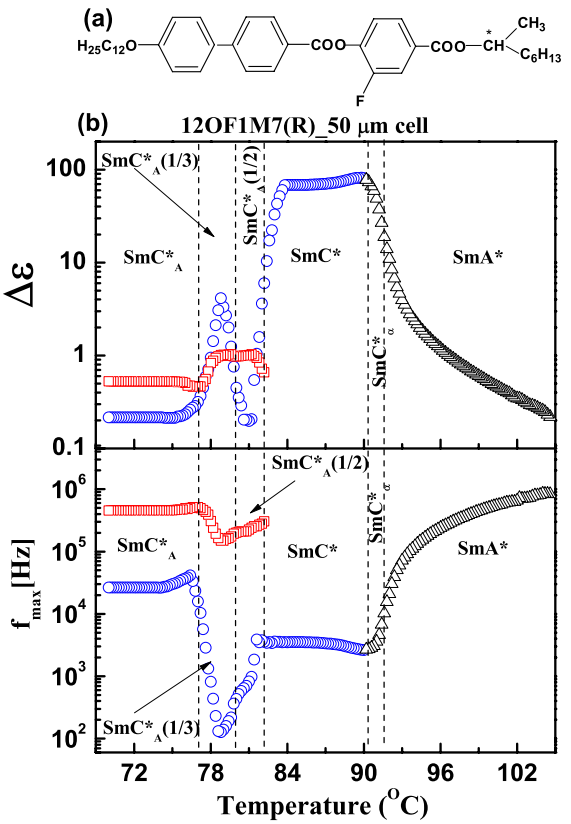

FIG. 2. (Color online) (a) Chemical structure of 12OF1M7(R). (b) Temperature dependence of dielectric strength ($\Delta\epsilon$) and relaxation frequency ($f_{\max}$) of different modes of the smectic-C^* variant phases for cell thickness of 50 μm for 12OF1M7(R).

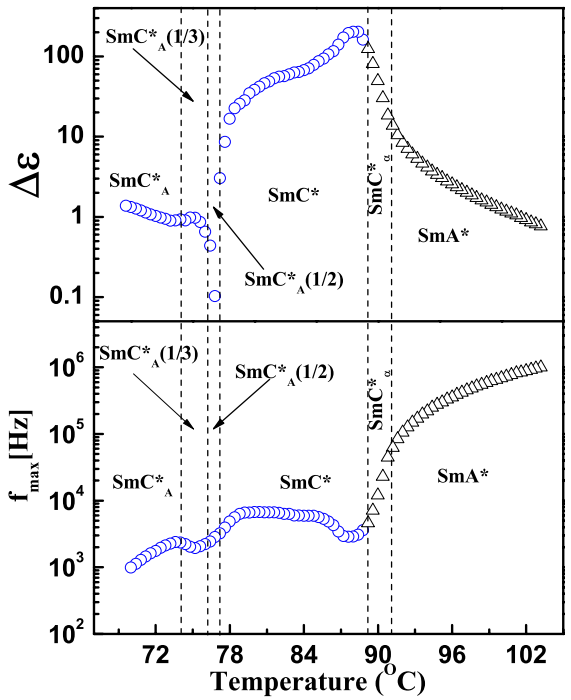

FIG. 3. (Color online) Temperature dependence of dielectric strength ($\Delta\epsilon$) and relaxation frequency (f_{max}) of different modes of the smectic-C^* variant phases for cell thickness of 10 μm for 12OF1M7(R).

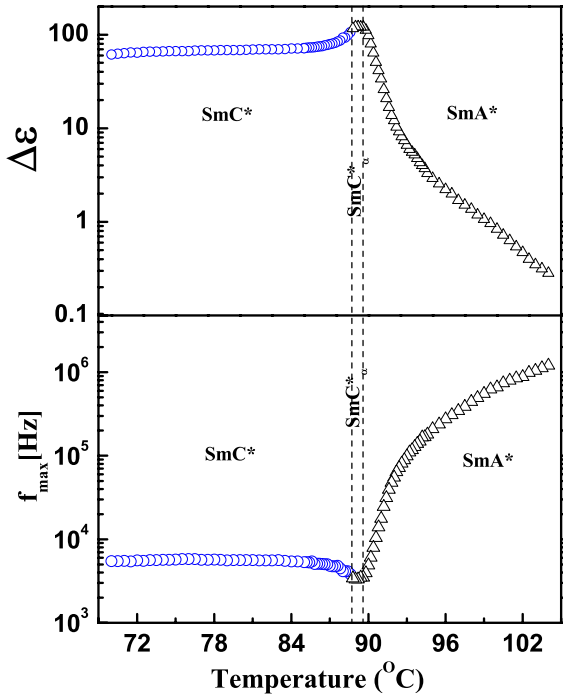

FIG. 4. (Color online) Temperature dependence of dielectric strength ($\Delta\epsilon$) and relaxation frequency (f_{max}) of different modes of the smectic-C^* variant phases for cell thickness of 3 μm for 12OF1M7(R).

III. RESULTS AND DISCUSSION

The model is experimentally verified using a prototype AFLC compound 12OF1M7(R) ((*R*)-(-)-1-methylhephtyl 4-(4'-dodecyloxybiphenyl-4-ylcarbonyloxy)-3-fluorobenzoate) (Kingston Chemicals, Hull, U.K.), chemical structure shown in Fig. 2(a). The experiments were performed on cooling the sample from 110 to 70 °C. Sample cells consisted of a planar capacitor made of two chemically etched indium tin oxide–coated glass plates with sheet resistance 20 Ω/□. For planar alignment, the conducting inner surfaces were spin coated with a polyimide RN 1175 (Nissan Chemicals, Japan) alignment layer and rubbed parallel. The cells were filled with the liquid crystals in the isotropic phase. Dielectric measurements in the frequency range from 1 Hz to 10 MHz were made by using the Novocontrol Alpha high-resolution dielectric analyzer with a rms voltage of 0.03 V. The thickness of the liquid crystal cell was measured based on the measurements of the transmittance spectra of an uv-visible spectrometer (AvaSpec-2048) using the interference fringes caused by the reflection from the two close glass surfaces of the cell.

The temperature dependence of dielectric strength ($\Delta\epsilon$) and relaxation frequency (f_{max}) for three different cell thicknesses of 50, 10, and 3 μm are shown in Figs. 2–4, respectively. These are found by fitting the imaginary part of the dielectric permittivity (ϵ'') to the Havriliak-Negami equation. The Havriliak-Negami equation for n relaxation processes is given by [32]

$$\epsilon^*(\omega) = \epsilon' - i\epsilon'' = \epsilon_\infty + \sum_{i=1}^{n} \frac{\Delta\epsilon_i}{[1+(j\omega\tau_i)^{\alpha_i}]^{\beta_i}} - \frac{j\sigma_{dc}}{\epsilon_0\omega}, \quad (12)$$

where ϵ_∞ is the high-frequency permittivity, i is a variable denoting the number of relaxation processes up to n, τ_i and $\Delta\epsilon_i$ are the relaxation time and the dielectric strength of the ith process, and α_i and β_i are the corresponding fitting parameters. The term $(-j\sigma_{dc}/\epsilon_0\omega)$ takes account of the dielectric loss due to ionic conduction. Ionic conduction is important at low frequencies. σ_{dc} is the dc conductivity, and ω and ϵ_0 are the angular frequency and the permittivity of the free space, respectively. The transition temperatures of different phases are determined by measuring $\Delta\epsilon$ and f_{max} of different collective and noncollective modes in the dielectric spectra over a wide range of frequency from 1 Hz to 10 MHz for eight different cells, thickness ranging from 3 to 80 μm as described below. In the SmA^* phase, the molecules in the planar configuration are parallel to the plane of the electrodes. The molecular relaxation mode around the long molecular axis (not shown) and the soft mode (black triangles) are both dielectrically active as the dipole moment normal to the electrodes fluctuates with electric field in this phase. Close to the transition temperature of the SmC^* phase, the soft mode dielectric strength sharply increases and the relaxation frequency sharply decreases. Based on this, the phase can therefore be easily identified as shown in Figs 2–4. In the SmC^* phase, the ferroelectric Goldstone mode (blue circles) is the most dominant and the phase is characterized mainly by this mode as shown in Figs. 2–4. The helix can easily be distorted by a weak external field and a change in the mac-

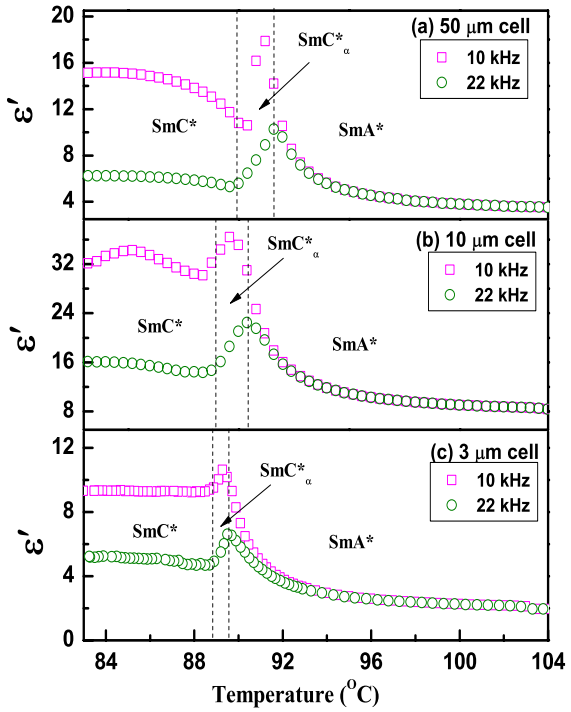

FIG. 5. (Color online) Temperature dependence of the real part of the dielectric permittivity (ϵ') in SmC^*_α phase for two frequencies of 10 and 22 kHz for cell thicknesses of 50 (a), 10 (b), and 3 μm (c) for 12OF1M7(R).

roscopic polarization with field is very significant and the relative permittivity is very large. Among the chiral smectic-C^* variant phases which have multilayer repeating units, the Sm$C^*_A(1/2)$ and SmC^*_A phases do not exhibit significant dielectric response due to the small macroscopic polarization, as the polarizations almost cancel out in the repeating units. The transition temperature from SmC^* to Sm$C^*(1/2)$ is determined by a drop in the dielectric strength. In Sm$C^*_A(1/3)$, on the other hand, the polarization is only partially canceled out and this phase thus exhibits a significant dielectric response. Due to its long helical pitch, the value of the relaxation frequency $f_{\max}$ in Sm$C^*_A(1/3)$ is much lower than in the SmC^* phase. The dielectric strength ($\Delta\epsilon$) is lower than in SmC^* due to the reduced macroscopic plarization. The transition temperature from Sm$C^*_A(1/2)$ to Sm$C^*_A(1/3)$ is determined by an increase in the dielectric strength and decrease in relaxation frequency, whereas the transition temperature from Sm$C^*_A(1/3)$ to SmC^*_A is determined by a drop in the dielectric strength and an increase in relaxation frequency for the low-frequency mode. Apart from the above discussed modes, several other modes appear in the bulk smectic-C^* variant phases as shown by red squares in Fig. 2 for the 50 μm cell. The characteristic dependence of the dielectric strength and frequency of the different modes for smectic-C^* variant phases is explained by Panarin *et al.* [33–35] in detail. The SmC^*_α phase is structurally equivalent to the SmC^* phase but has an extremely short pitch compared to SmC^*. This is characterized by a change in the slope of the real part of the permittivity (ϵ') as a function of temperature [36] shown in Fig. 5 for 50 (a), 10 (b), and 3 μm (c) cells for frequencies of 10 and 22 kHz. The first change in the slope is due to an increase in the amplitude of the soft mode close to the SmA to SmC^*_α transition, and the second is due to a decrease in the strength of soft mode followed by an increase in the strength of the Goldstone mode at the SmC^*_α to SmC^* transition. Note that for the 10 μm cell a surface-induced mode appears, which is not a characteristic of the phase but is a result of the influence of the cell substrate. This along with the soft mode results in an increased dielectric strength at the SmC^*_α to SmC^* transition compared to that for a 50 μm cell.

We note from Figs. 2–5 that the temperature ranges of SmC^*_α, Sm$C^*_A(1/2)$, and Sm$C^*_A(1/3)$ phases are narrower for the 10 μm than for the 50 μm cell. Furthermore, Sm$C^*_A(1/2)$ and Sm$C^*_A(1/3)$ are completely suppressed by a thin cell of 3 μm thickness. Figures 6(a) and 6(b) show the experimental results for the dependence of the transition temperatures of the phases and the temperature range for which the phases: SmC^*_α, Sm$C^*_A(1/2)$, and Sm$C^*_A(1/3)$ are stable, with the cell thickness varying from 3 to 80 μm. We note that the transition temperatures of almost all phases show a decreasing trend with decreasing cell thicknesses. We find that, on reducing the cell thickness, the Sm$C^*_A(1/2)$ phase disappears prior to the Sm$C^*_A(1/3)$ phase, whereas the SmC^*_α phase is rather stable. For cell thicknesses greater than 10 μm, the temperature ranges of the phases do not vary to a large extent, whereas for smaller cell thicknesses, the temperature ranges of the phases decrease rapidly on decreasing the cell thickness, to the extent that for a thickness 3 μm Sm$C^*_A(1/2)$ and Sm$C^*_A(1/3)$ totally disappear. Figures 6(c) and 6(d) show the plots of the calculated results from the theoretical model. Here, we may assert that exact determination of the phase transition temperature is rather difficult since the phase transition occurs gradually as the cell thickness is reduced. The phase transition temperatures are also influenced by the coexistence of phases. The results presented in Fig. 6 are presented for understanding the qualitative behavior of the stability of the smectic-C^* variant phases as a function of the cell thickness. Moreover, we also point out that the experiments are carried out during cooling of the sample; the results therefore include the supercooling effect. On the contrary the theory given here excludes the supercooling effect. The intrinsic phase transition temperature, which is usually represented as T_c, is different from the actual transition temperature (represented as T_0) for a first-order transition. T_c is the temperature where the free energy of the two phases becomes the same, and T_0 is the temperature where the phase transition occurs when the supercooling effect is included. Most phenomenological models for the transitions between the tilted smectic phases aim to find T_c, ignoring the supercooling effect, though the supercooling is actually very large, especially for thin cells. Our theory also focuses on finding T_c. Note that the supercooling in the phase transitions between tilted smectics is rather different from the conventional concept of supercooling, because in the tilted smectics it is governed mostly by the surface effects, while normally it is governed by the free energy barrier between the two phases. This is the case for most phenomenological theories. This is one of the main reasons for the slight disagreement

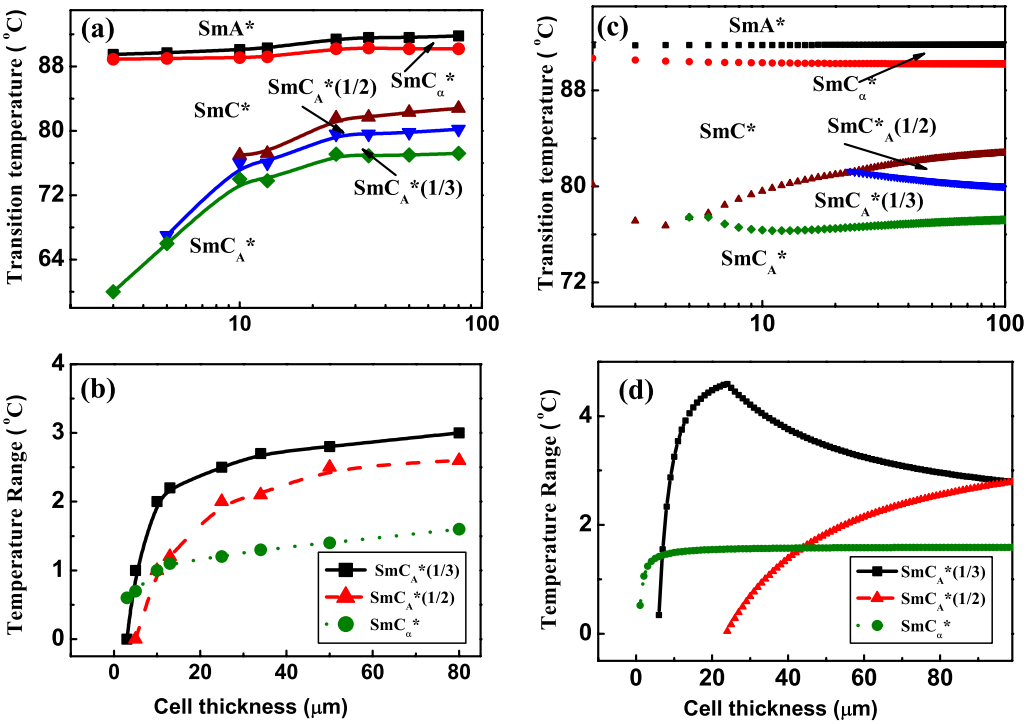

FIG. 6. (Color online) The dependence of the (a) transition temperature of the phases and (b) temperature range for which SmC^*_α, Sm$C^*_A(1/2)$ and Sm$C^*_A(1/3)$ phases are stable as a function of the cell thickness that varies from 3 to 80 μm. (c–d) represents the calculated results under the condition: $w_1/A_0=5.5\times10^6$ m.

between experimental and theoretical results presented in Figs. 6(a)–6(d), apart from the simplifications made in the theoretical calculations. Therefore, as the thickness of the cell is reduced, the experimentally measured transition temperatures may be further reduced due to the supercooling effect [19]. Since supercooling may occur for all the phases, the temperature range for the stability of each phase may not be affected by this effect. However, the theoretical results are in good qualitative agreement with the experiments considering the significant simplifications made in the calculations. For the Sm$C^*_A(1/3)$ data in Fig. 6(d), we note that the temperature range of the Sm$C^*_A(1/3)$ phase is rather constant up to the cell thickness where the Sm$C^*_A(1/2)$ disappears, and then sharply decreases on decreasing the cell thickness. A similar two-step stability appears in the experimental results as shown in Fig. 6(b).

The suppression of these phases on decreasing cell thickness was also observed by Lagerwall *et al.* [19,20]. Hiraoka *et al.* [23] found that the temperature range of the Sm$C^*_A(1/2)$ phase increases on decreasing the cell thickness, which is different from our results. This is because, in their material, SmC^* phase is not present, and while the transition temperature between the SmC^*_α and Sm$C^*_A(1/2)$ phases is not significantly affected, as explained, the transition between the Sm$C^*_A(1/2)$ and Sm$C^*_A(1/3)$ phases decreases with cell thickness due to the supercooling effect. Hence, the temperature range of the Sm$C^*_A(1/2)$ phase increases but this does not contradict the theory. Note that the Sm$C^*_A(1/2)$ and Sm$C^*_A(1/3)$ phases disappear when the cell thickness is decreased further [23]. Panarin *et al.* [27] observed suppression of the subphases by confinement, as w_1 is weak in all SmC^* variant phases of their experiment because the cell surfaces were not coated with a polymer, Sm-C^* variant phases therefore are shown to exist down to much lower cell thicknesses than is the case here where the surfaces are coated by a polymer.

IV. CONCLUSIONS

In summary, the stability of SmC^*_α, Sm$C^*_A(1/2)$, Sm$C^*_A(1/3)$, and SmC^*_A phases is investigated by determining the transition temperatures and the temperature range for which they are stable by varying the cell thickness experimentally. A simple theory has explained the experimental observations. (i) Sm$C^*_A(1/3)$ is more stable than Sm$C^*_A(1/2)$ when the effect due to surfaces is included. This is because Sm$C^*_A(1/2)$ has a higher anchoring energy compared to the adjacent phases due to the absence of polar anchoring energy. (ii) The stability is mostly due to a large polar anchoring strength with large spontaneous polarization and a consequent reduction in the surface energy. (iii) SmC^*_α is rather stable, and the transition temperatures between the higher-temperature phases are unaffected by the surfaces. This arises from the higher temperature-dependent coefficient of the free energy. (iv) The temperature range of Sm$C^*_A(1/3)$ is rather constant up to the thickness for which Sm$C^*_A(1/2)$ exists. Once Sm$C^*_A(1/2)$ disappears, the temperature range of Sm$C^*_A(1/3)$ decreases rapidly on decreasing the cell thickness.

ACKNOWLEDGMENTS

SFI Grant No. (02/IN.1.I.031) is thanked for funding the research work. One of the authors (JKS) thanks Samsung Electronics Co. Ltd for granting a leave of absence from Seoul. We thank Atsuo Fukuda for fruitful discussions.

[1] A. D. L. Chandani, Y. Ouchi, H. Takezoe, A. Fukuda, K. Terashima, K. Furukawa, and A. Kishi, Jpn. J. Appl. Phys., Part 2 **28**, L1261 (1989).
[2] A. D. L. Chandani, E. Gorecka, Y. Ouchi, H. Takezoe, and A. Fukuda, Jpn. J. Appl. Phys., Part 2 **28**, L1265 (1989).
[3] N. Okabe, Y. Suzuki, I. Kawamura, T. Isozaki, H. Takezoe, and A. Fukuda, Jpn. J. Appl. Phys., Part 2 **31**, L793 (1992).
[4] E. Gorecka, A. D. L. Chandani, Y. Ouchi, H. Takezoe, and A. Fukuda, Jpn. J. Appl. Phys., Part 1 **29**, 131 (1990).
[5] H. Takezoe, J. Lee, Y. Ouchi, and A. Fukuda, Mol. Cryst. Liq. Cryst. **202**, 85 (1991).
[6] A. D. L. Chandani, N. M. Shtykov, V. P. Panov, A. V. Emelyanenko, A. Fukuda, and J. K. Vij, Phys. Rev. E **72**, 041705 (2005).
[7] V. P. Panov, J. K. Vij, Yu. P. Panarin, C. Blanc, V. Lorman, and J. W. Goodby, Phys. Rev. E **75**, 042701 (2007).
[8] H. Orihara and I. Ishibashi, Jpn. J. Appl. Phys., Part 2 **29**, L115 (1990).
[9] B. Zeks and M. Cepic, Liq. Cryst. **14**, 445 (1993).
[10] A. Fukuda, Y. Takanishi, T. Isozaki, K. lshikawa, and H. Takezoe, J. Mater. Chem. **4**, 997 (1994).
[11] A. Roy and N. V. Madhusudana, Europhys. Lett. **36**, 221 (1996).
[12] T. Akizuki, K. Miyachi, Y. Takanishi, K. Ishikawa, H. Takezoe, and A. Fukuda, Jpn. J. Appl. Phys., Part 1 **38**, 4832 (1999).
[13] P. M. Johnson, D. A. Olson, S. Pankratz, T. Nguyen, J. Goodby, M. Hird, and C. C. Huang, Phys. Rev. Lett. **84**, 4870 (2000).
[14] A. V. Emelyanenko and M. A. Osipov, Phys. Rev. E **68**, 051703 (2003).
[15] M. A. Osipov, A. Fukuda, and H. Hakoi, Mol. Cryst. Liq. Cryst. **402**, 9 (2003).
[16] M. Cepic and B. Zeks, Mol. Cryst. Liq. Cryst. Sci. Technol., Sect. A **263**, 61 (1995).
[17] T. Isozaki, F. Takayuki, H. Takezoe, A. Fukuda, T. Hagiwara, Y. Suzuki, and I. Kawamura, Jpn. J. Appl. Phys., Part 2 **31**, L1435 (1992).
[18] D. W. Berreman, Phys. Rev. Lett. **28**, 1683 (1972).
[19] J. P. F. Lagerwall, D. D. Parghi, D. Kruerke, F. Gouda, and P. Jagemalm, Liq. Cryst. **29**, 163 (2002).
[20] J. P. F. Lagerwall, P. Rudquist, S. T. Lagerwall, and B. Stebler, Ferroelectrics **277**, 239 (2002).
[21] P. Jagemalm, J. P. F. Lagerwall, A. Dahlgren, L. Komitov, A. S. Matharu, C. Grover, F. Gouda, and A. A. Kutub, Ferroelectrics **244**, 147 (2000).
[22] H. Moritake, N. Shigeno, M. Ozaki, and K. Yoshino, Liq. Cryst. **14**, 1283 (1993).
[23] K. Hiraoka, T. Maruyama, and Y. Noguchi, Jpn. J. Appl. Phys., Part 1 **43**, 8173 (2004).
[24] Yu. P. Panarin, C. Rosenblatt, and F. M. Aliev, Phys. Rev. Lett. **81**, 2699 (1998).
[25] H. Xu, J. K. Vij, A. Rappaport, and N. A. Clark, Phys. Rev. Lett. **79**, 249 (1997).
[26] J.-F. Li, E. A. Shack, Y.-K. Yu, X.-Y. Wang, C. Rosenblatt, M. E. Neubert, S. S. Keast, and H. Gleeson, Jpn. J. Appl. Phys., Part 2 **35**, L1608 (1996).
[27] Yu. P. Panarin, Yu. P. Kalmykov, S. T. MacLughadha, H. Xu, and J. K. Vij, Phys. Rev. E **50**, 4763 (1994).
[28] W. Chen, M. B. Feller, and Y. R. Shen, Phys. Rev. Lett. **63**, 2665 (1989).
[29] M. A. Handschy, N. A. Clark, and S. T. Lagerwall, Phys. Rev. Lett. **51**, 471 (1983).
[30] M. Brunet and E. Williams, Ann. Phys. (N.Y.) **3**, 237 (1977).
[31] M. Glogarova, J. Fousek, L. Lejek, and J. Pavel, Ferroelectrics **58**, 161 (1984).
[32] S. Havriliak, Jr. and S. Negami, Polymer **8**, 161 (1967).
[33] Yu. P. Panarin, O. Kalinovskaya, J. K. Vij, and J. W. Goodby, Phys. Rev. E **55**, 4345 (1997).
[34] Yu. P. Panarin, O. Kalinovskaya, and J. K. Vij, Liq. Cryst. **25**, 241 (1998).
[35] Yu. P. Panarin, O. Kalinovskaya, and J. K. Vij, Appl. Phys. Lett. **72**, 1667 (1998).
[36] N. M. Shtykov, J. K. Vij, V. P. Panov, R. A. Lewis, M. Hird, and J. W. Goodby, J. Mater. Chem. **9**, 1383 (1999).